

Supplementary Information

Self-Assembled Tetracyanoquinodimethane Derivatives: Differential Fluorescent Responses on Sensing Copper and Mercury Ions in Aqueous Medium

Anuradha Sureshrao Mohitkar,^a Nilanjan Dey^b and Subbalakshmi Jayanty^{c*}

^{a,b,c} Department of Chemistry, Birla Institute of Technology and Science, Pilani-Hyderabad Campus, Jawaharnagar, Kapra Mandal, Hyderabad - 500078, Telangana State, India.

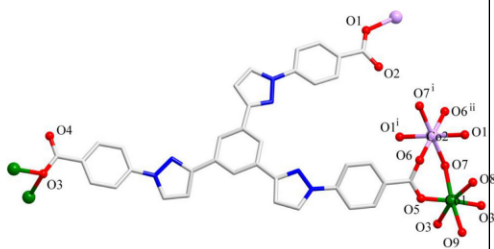
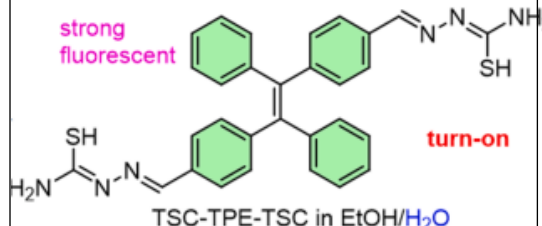
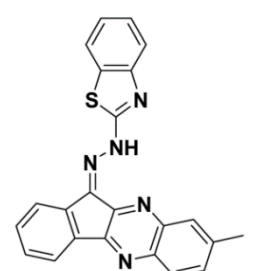
Correspondence e-mail: jslakshmi@hyderabad.bits-pilani.ac.in

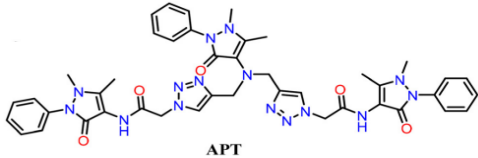
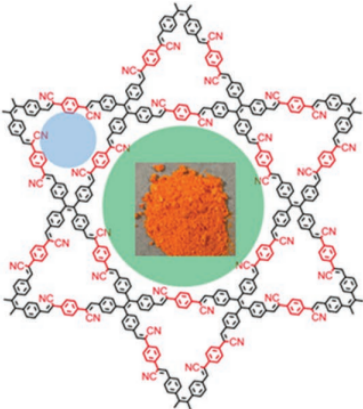
S: *Supplementary information*

Table of Contents

Contents	Page No.
Table S1 (a) Comparative table of fluorescent probe with varying parameters against metal ion sensing.	S3-S4
Fig. S1 (a) Increase of emission intensity with the increase in water fraction (b) effect of viscosity on intensity (c) effect of temperature for [1] .	S5
Fig. S2 (a) Lowering of emission intensity with the decrease in concentration (b) effect of pH on intensity (c) SEM image for [1] .	S6
Fig. S3 [2] (a) Absorption spectra and (b) emission spectra ($\lambda_{exc} = 370$ nm) depicting solvatochromism (c) effect of aggregation on emission intensity, (d) lowering of emission intensity with the decrease in concentration.	S7
Fig. S4 [3] (a) Absorption spectra and (b) emission spectra ($\lambda_{exc} = 375$ nm) depicting solvatochromism (c) effect of aggregation on emission intensity, (d) lowering of emission intensity with the decrease in concentration.	S8
Fig. S5 Emission intensity changes with effect of (a) temperature and (b) pH (c) SEM image for [2] .	S9
Fig. S6 Emission intensity changes with effect of (a) temperature and (b) pH (c) SEM image for [3] .	S10
Fig. S7 Variation in emission intensity of [2] with increase in (a) Cu^{2+} and (b) Hg^{2+} . Change in absorbance with increase in concentration of (c) Cu^{2+} and (d) Hg^{2+} for [2] .	S11
Fig. S8 Variation in emission intensity of [3] with increase in (a) Cu^{2+} and (b) Hg^{2+} . Change in absorbance with increase in concentration of (c) Cu^{2+} and (d) Hg^{2+} for [3] .	S12
Fig. S9 (a) Stern-Volmer plot, (b) K_{sv} calculation, (c) LOD calculation, depicting quenching of [1] on addition of Cu^{2+} ion.	S13
Fig. S10 Stern-Volmer plots for (a) Cu^{2+} and (b) Hg^{2+} , K_{sv} calculation (c) Cu^{2+} and (d) Hg^{2+} , LOD calculation (e) Cu^{2+} and (f) Hg^{2+} , for [2] .	S14
Fig. S11 Stern-Volmer plots for (a) Cu^{2+} and (b) Hg^{2+} , K_{sv} calculation (c) Cu^{2+} and (d) Hg^{2+} , LOD calculation (e) Cu^{2+} and (f) Hg^{2+} for [3] .	S15
Fig. S12 (a) 1H NMR and (b) IR spectra showcasing the effect of metal ions on [2] .	S16
Fig. S13 (a) 1H NMR and (b) IR spectra showcasing the effect of metal ions on [3] .	S17
Fig. S14 EDAX (a) spectra showing elemental composition and (b) mapping depicting elemental presence for [1] .	S18-S19
Fig. S15 EDAX (a) spectra showing elemental composition and (b) mapping depicting elemental presence for [2] .	S20-S21
Fig. S16 EDAX (a) spectra showing elemental composition and (b) mapping depicting elemental presence for [3] .	S22-S23
Fig. S17 Variation in emission intensity of [1] against Cu^{2+} ions with (a) pond water sample and (b) tap water sample.	S24

Table S1 Comparative table for fluorescent probes with respect to synthesis condition, sensing ions, detection method, LOD, solvent medium.

Fluorescent Probe	Synthesis Condition	Sensing Ions & Detection Method	LOD (M)	Solvent Medium	References
<p>[Co3(L)2(H2O)6]n (1) L= 1,3,5-(tris(1-(4- carboxyphenyl)-1h-pyrazol-3-yl) benzene (H3L)</p> 	<p>In autoclave Temperature :140 °C, Time : 72 h, Multistep synthesis</p>	<p>Cu²⁺ Fluorescence (Quenching)</p> <p>Hg²⁺ Fluorescence (Quenching)</p>	<p>Cu²⁺ 9.91 × 10⁻⁷</p> <p>Hg²⁺ 1.26 × 10⁻⁵</p>	<p>N,N-dimethylacetamide (DMA)</p>	<p>[1]</p>
<p>2-(4-Bromophenyl)ethene-1,1,2-triyltribenzene (2) and 4-(1,2,2-triphenylvinyl)benzaldehyde</p> 	<p>Temperature : -78 °C, Time : 48 h, Multistep synthesis</p>	<p>Cu²⁺ Fluorescence (Quenching)</p> <p>Hg²⁺ Fluorescence (Quenching)</p>	<p>Cu²⁺ 2.42 × 10⁻⁶</p> <p>Hg²⁺ 0.39 × 10⁻⁶</p>	<p>EtOH/H2O (v/v:1/1)</p>	<p>[2]</p>
<p>Quinoxaline-hydrazinobenzothiazole</p> 	<p>Temperature : 70 °C, Time : 12 h, Multistep synthesis</p>	<p>Cu²⁺ Fluorescence (Enhancement)</p> <p>Co²⁺ Fluorescence (Enhancement)</p> <p>Ni²⁺ Fluorescence (Enhancement)</p> <p>Hg²⁺ Fluorescence (Enhancement)</p>	<p>Cu²⁺ 1.16 × 10⁻⁷</p> <p>Hg²⁺ 1.14 × 10⁻⁷</p>	<p>THF : H2O (1 : 9, v/v) (pH 7.4, 20 mM HEPES buffer)</p>	<p>[3]</p>

4-amino antipyrine linked bis-1,2,3-triazole  APT	Temperature : RT, Time : 18 h, Multistep synthesis	Cu ²⁺ Absorbance (Enhancement) Hg ²⁺ Absorbance (Enhancement)	Cu ²⁺ 63 × 10 ⁻⁶ Hg ²⁺ 56 × 10 ⁻⁶	DMSO	[4]
Tetraphenylethylene (TPE) based COF nanosheets 	Temperature : 120 °C, Time : 5 days, Multistep synthesis	Cu ²⁺ Fluorescence (Quenching)	0.28 × 10 ⁻⁹	Neutral F127 surfactant in aqueous media	[5]
This Work	Temperature : 75 °C, Time: 3 h, Simple single step synthesis	Cu ²⁺ Fluorescence (Quenching) Hg ²⁺ Fluorescence (Quenching in case of [2,3] and enhancement in [1])	Cu ²⁺ 0.751 × 10 ⁻⁶ Hg ²⁺ 3.1937 × 10 ⁻⁶	MeCN: H ₂ O (1:9)	

References

1. Y. Xi, M. Hua , L. Gao, Q. Sun , E. Ma , W. Hu , M. Li , W. Liu , J. Sun and C. Zhang, *J. Mol. Struct.*, 2023, **1284**, 135456.
2. S. Bayindir , A. S. Hussein, F. Lafzi and M. Toprak, *J. Mol. Liq.*, 2023, **382**, 121939.
3. D. B. C. Leslee, U. Venkatachalam, J. Gunasekaran, S. Karuppannan and S. Bharathi Kuppannan, *Org. Biomol. Chem.*, 2023, **21**, 4130–4143.
4. S. Kumar, B. Lal, R. K. Tittal, G. Singh, J. Singh, G. Vikas D, R. Sharma and J. K. Sabane *Sens. Diagn.*, 2023, **2**, 1267–1276.
5. Zi. Yan, L. Fang, Z. He, H. Xie, B. Liu , B. Guo and Y. Yao, *Small*, 2022, **18**, 2200388.

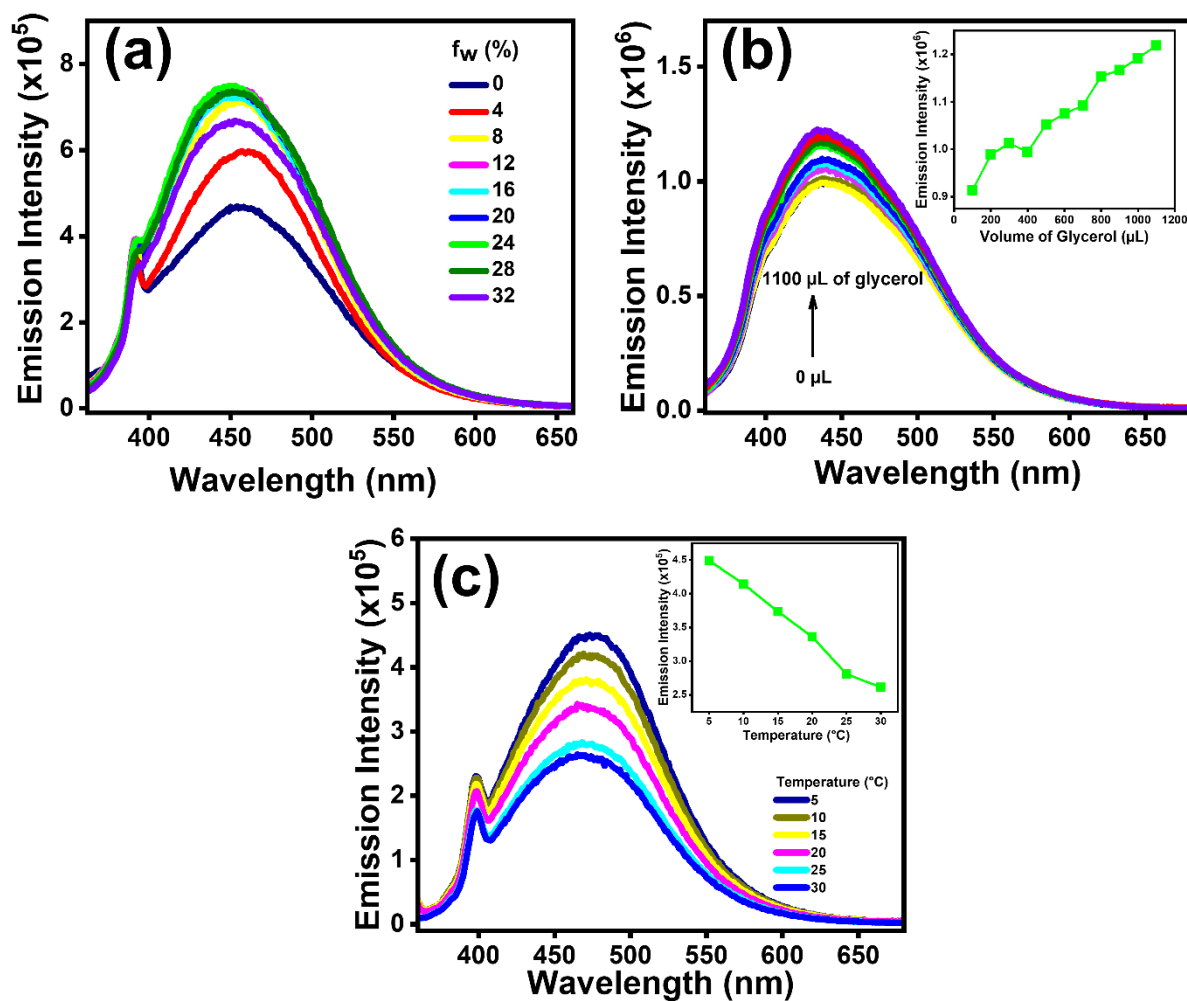


Fig. S1 (a) Increase of emission intensity with the increase in water fraction, (b) enhanced emission intensity with higher viscosity, (c) decrease in emission intensity with higher temperature for [1].

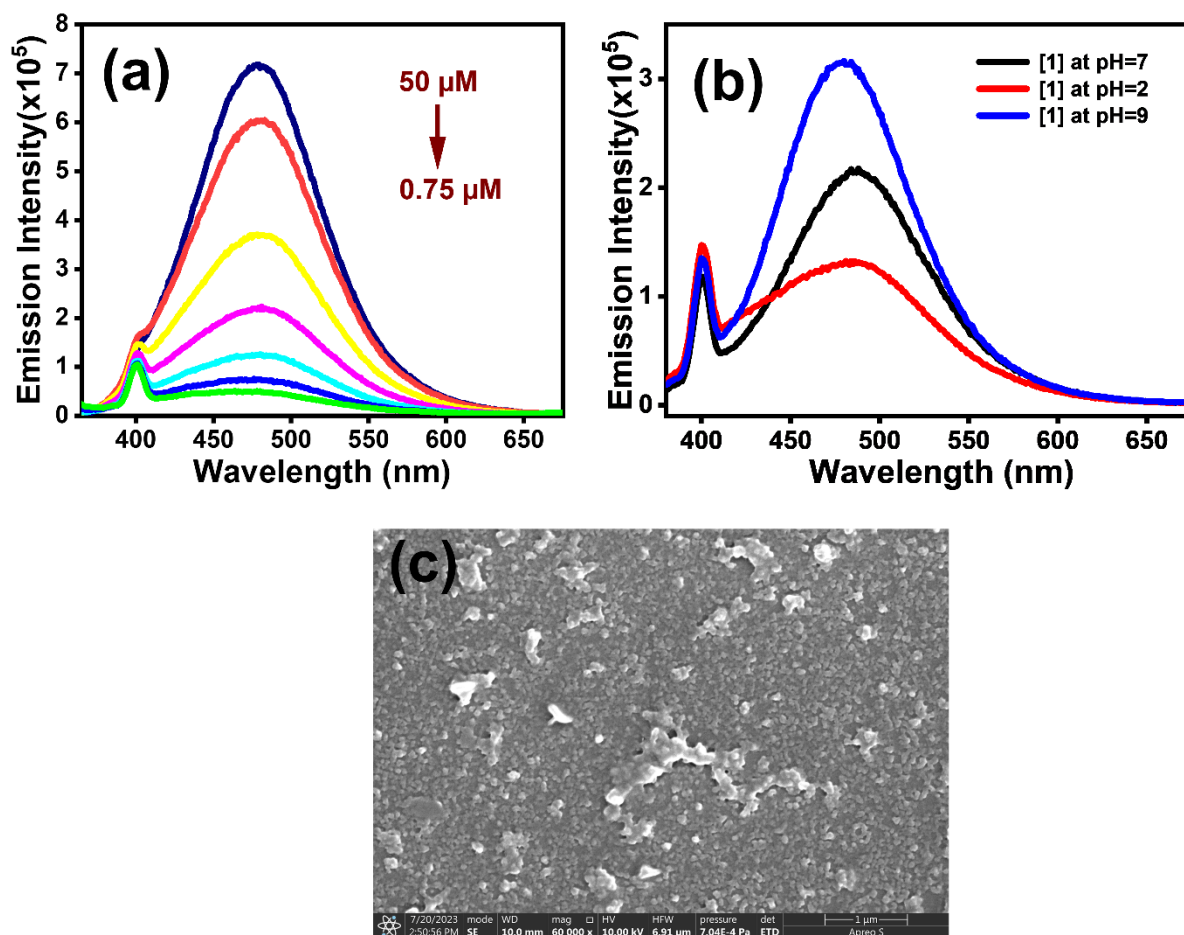


Fig. S2 (a) Lowering of emission intensity with the decrease in concentration, (b) enhanced emission intensity with higher pH, (c) formation of aggregates observed in SEM image for **[1]**.

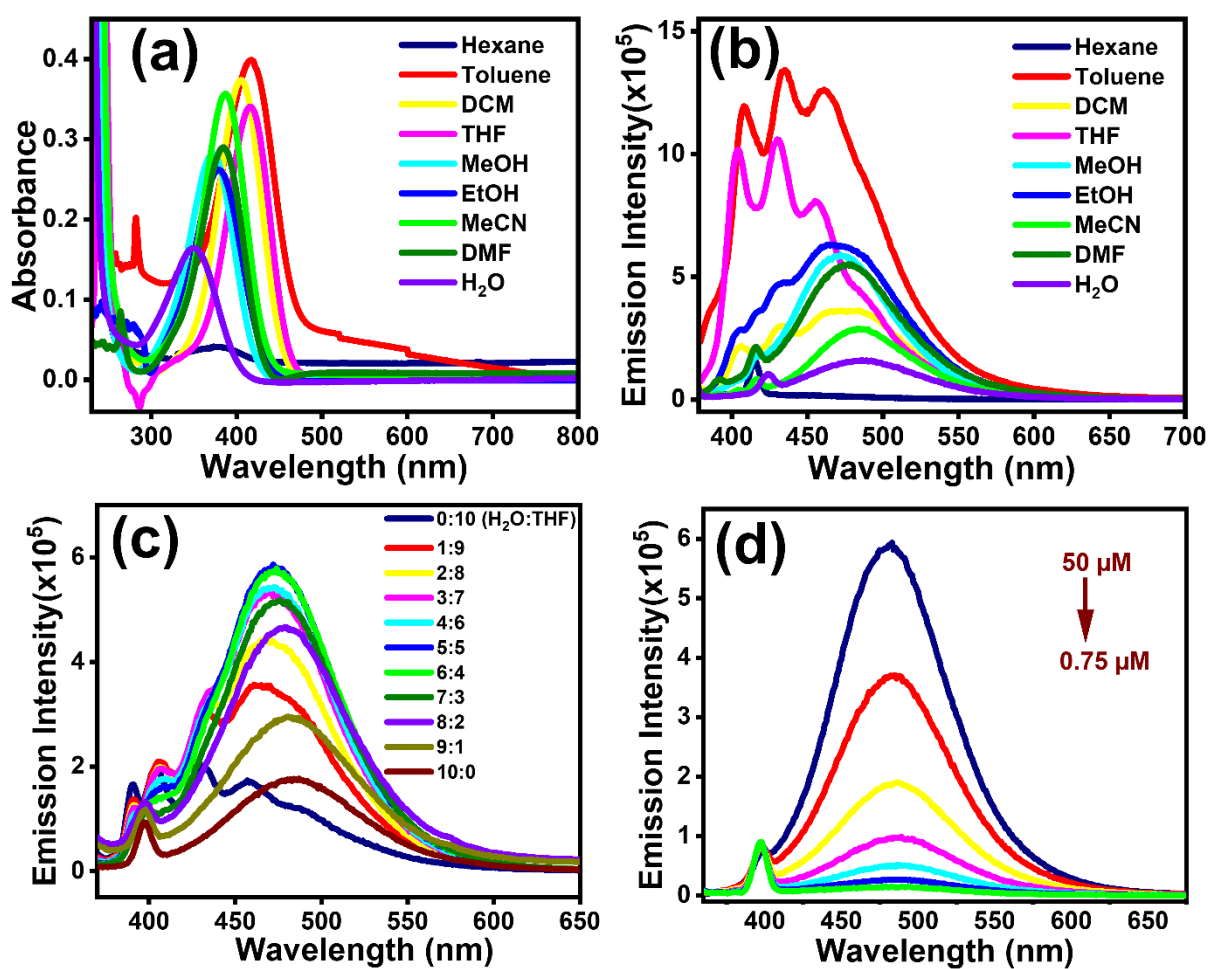


Fig. S3 [2] (a) Shift in absorption spectra and (b) emission spectra ($\lambda_{\text{exc}} \sim 370$ nm) with increase in polarity depicting solvatochromism, (c) quenching of emission intensity due to aggregation in varying proportions of H₂O:THF solvent mixture, (d) lowering of emission intensity with the decrease in concentration.

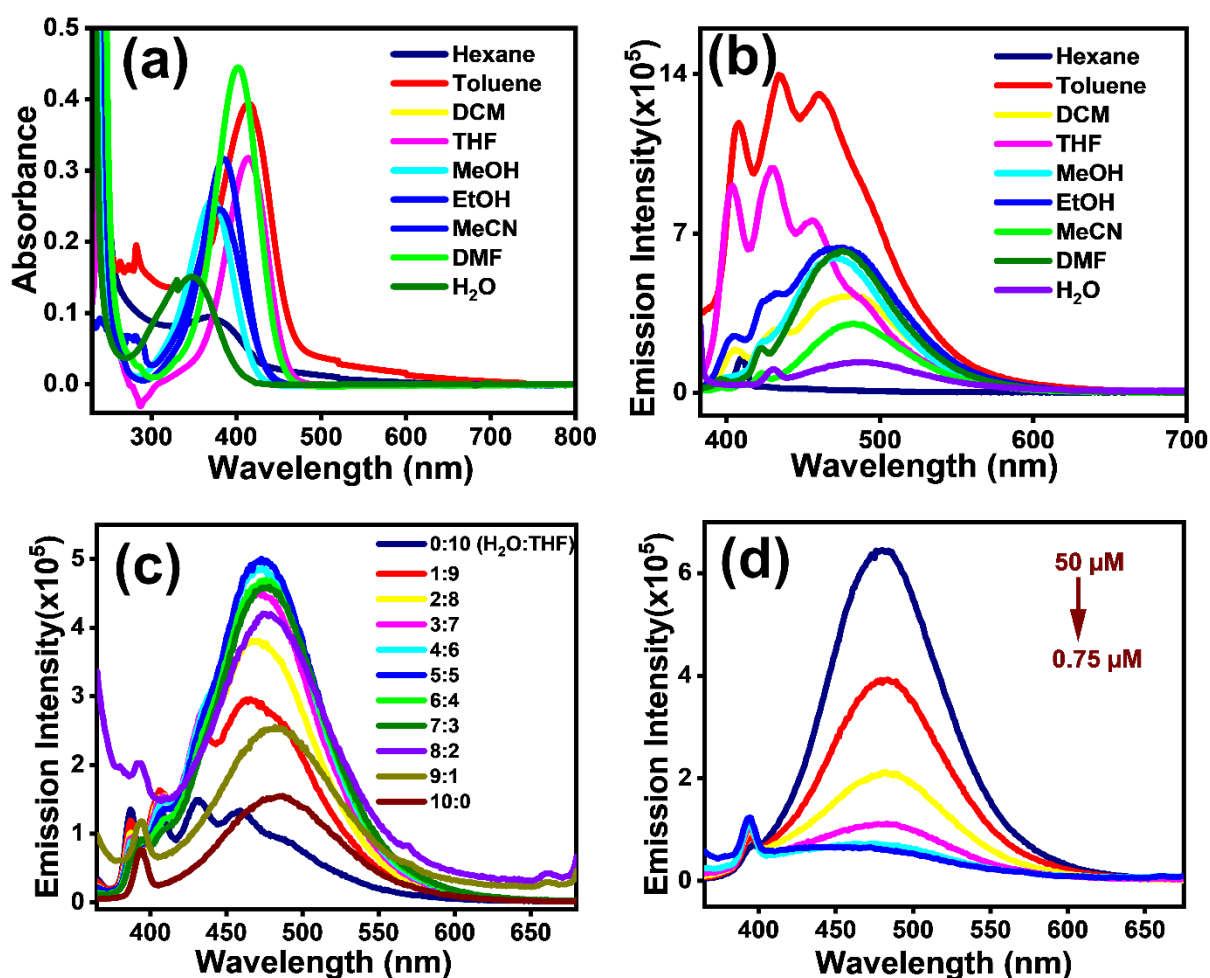


Fig. S4 [3] (a) Shift in absorption spectra and (b) emission spectra ($\lambda_{\text{exc}} \sim 375$ nm) with increase in polarity depicting solvatochromism, (c) quenching of emission intensity due to aggregation in varying proportions of H₂O:THF solvent mixture, (d) lowering of emission intensity with the decrease in concentration.

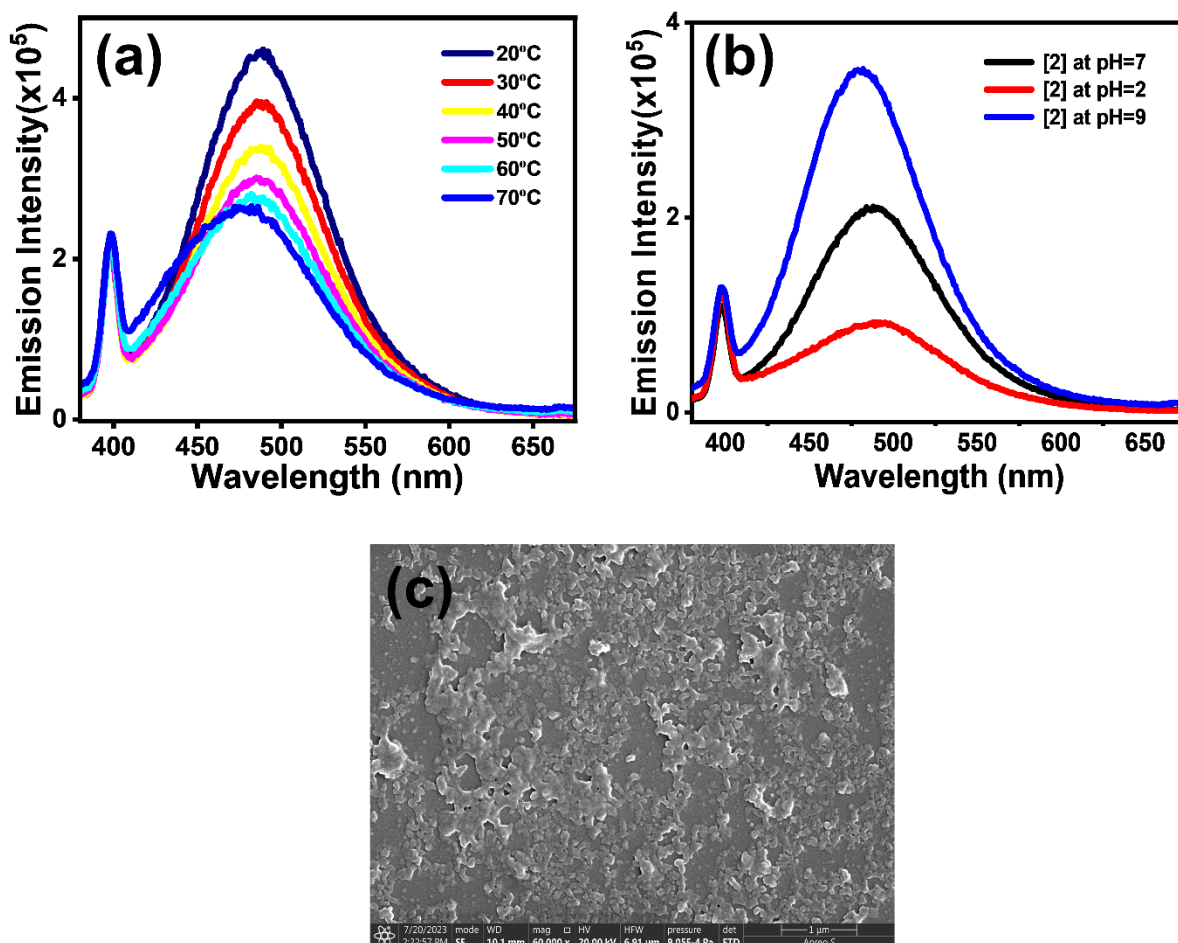


Fig. S5 (a) Lowering of emission intensity with the increase in temperature, (b) enhanced emission intensity with higher pH, (c) formation of aggregates observed in SEM image for [2].

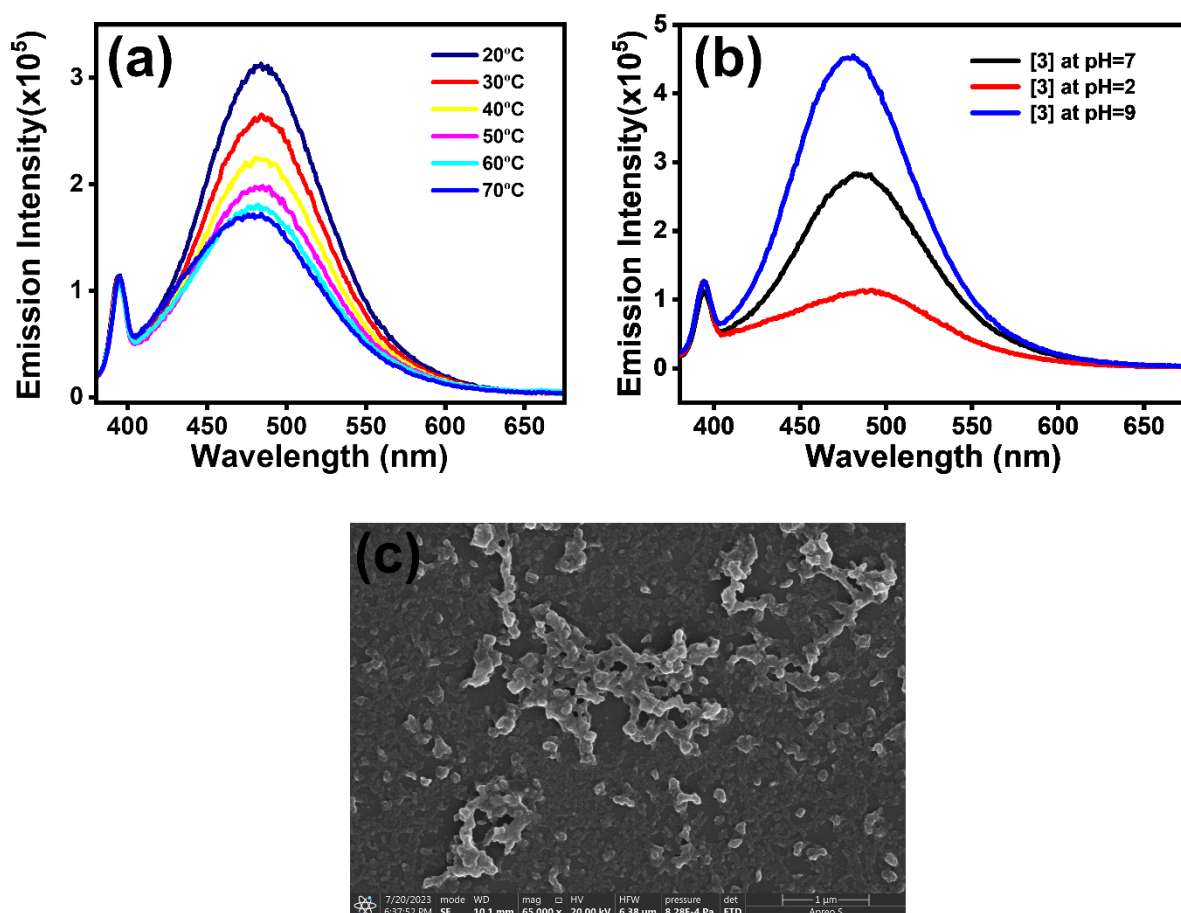


Fig. S6 (a) Lowering of emission intensity with the increase in temperature, (b) enhanced emission intensity with higher pH, (c) formation of aggregates observed in SEM image for [3].

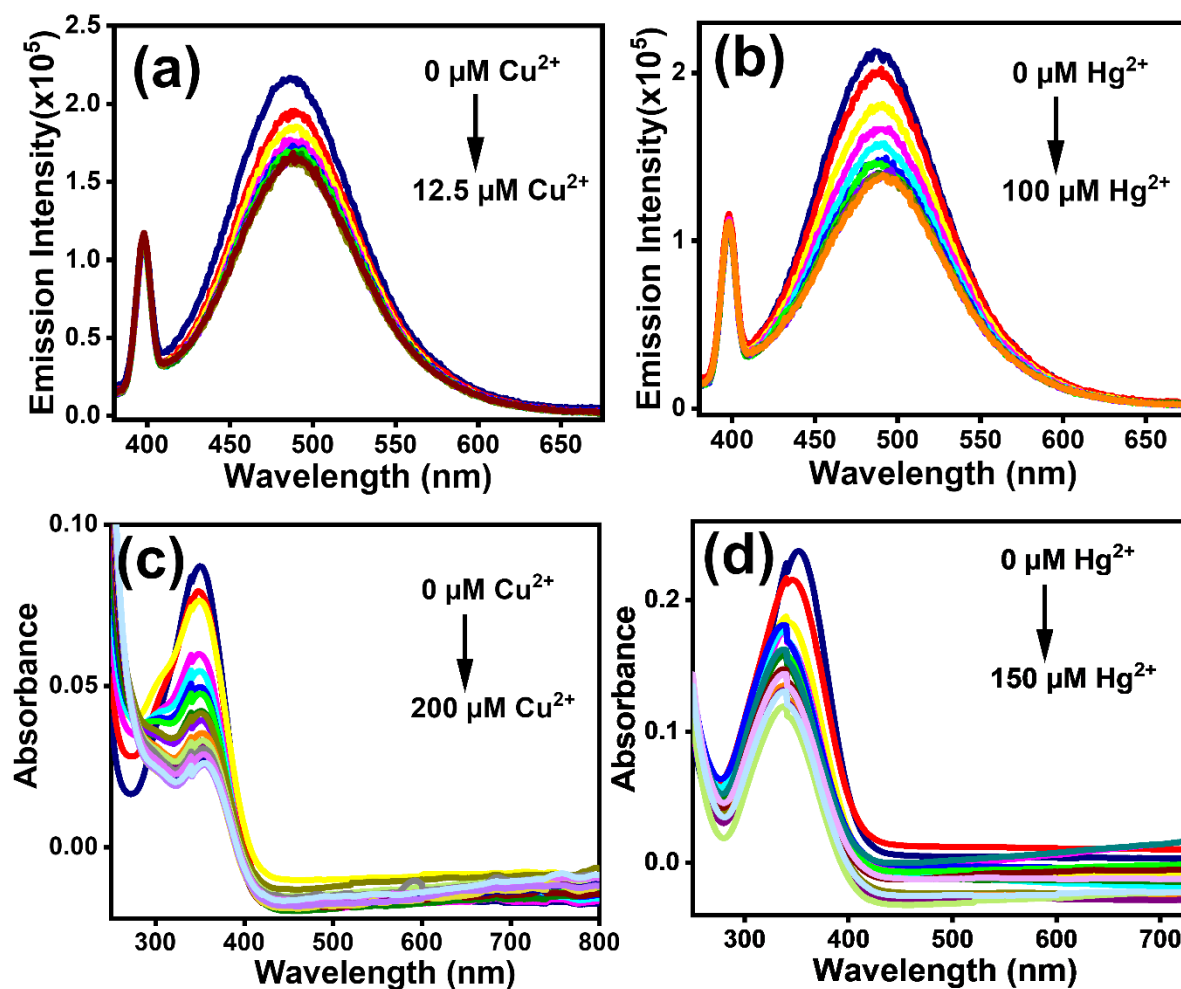


Fig. S7 Variation in emission intensity of **[2]** with increase in metal ion concentration: quenching effect for (a) Cu^{2+} and (b) Hg^{2+} . Lowering of absorbance with an increase in concentration of (c) Cu^{2+} and (d) Hg^{2+} for **[2]**.

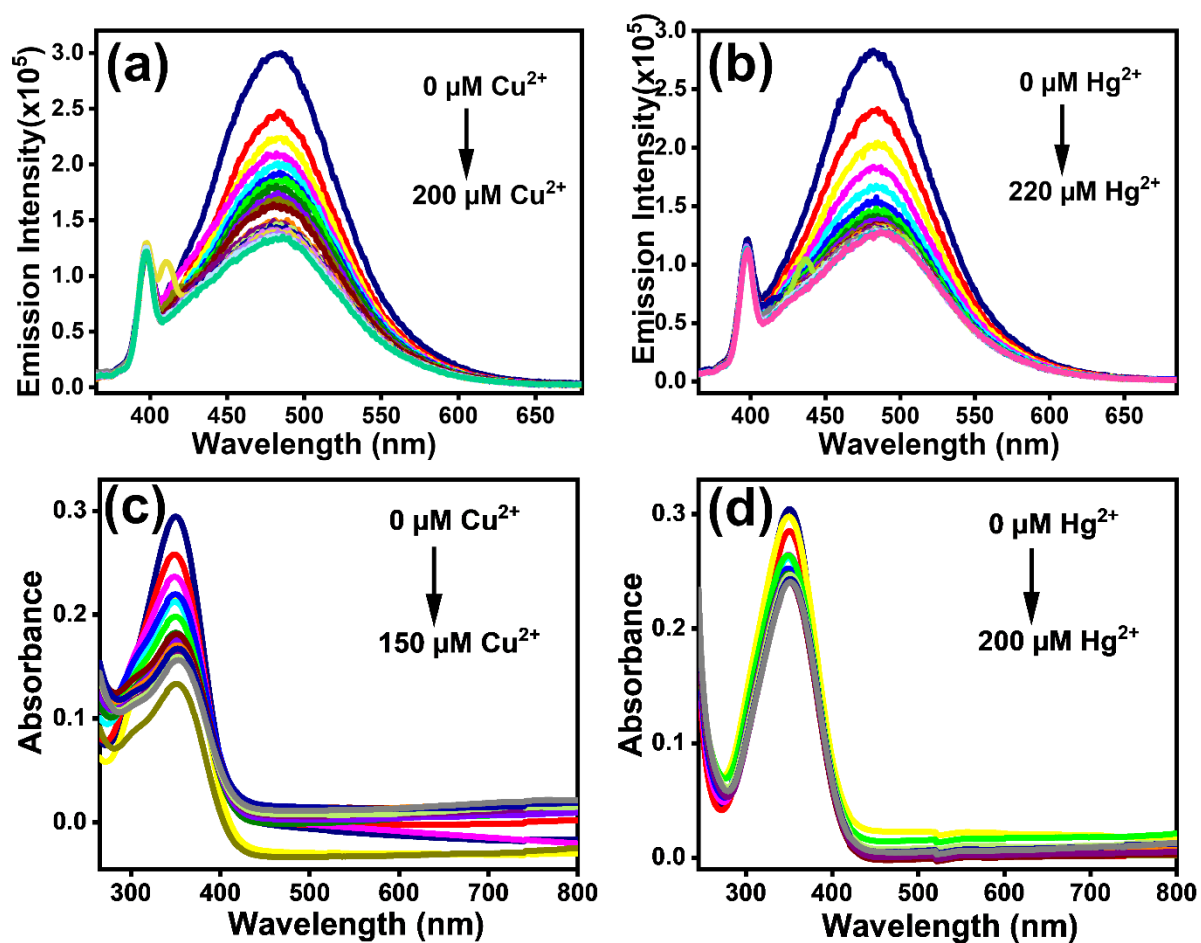


Fig. S8 Variation in emission intensity of **[3]** with increase in metal ion concentration: quenching effect for (a) Cu^{2+} and (b) Hg^{2+} . Lowering of absorbance with an increase in concentration of (c) Cu^{2+} and (d) Hg^{2+} for **[3]**.

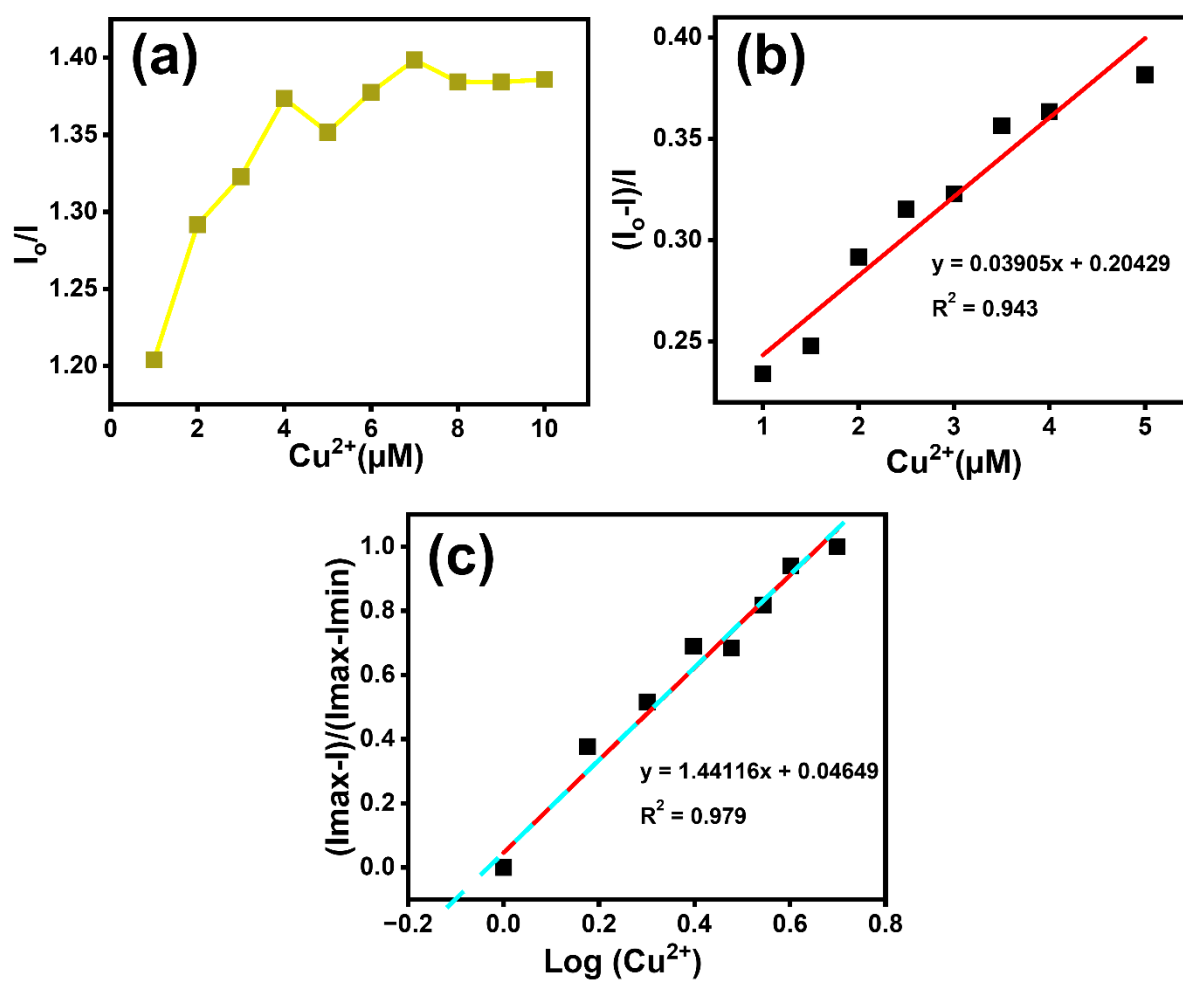


Fig. S9 (a) Stern-Volmer plot, (b) K_{sv} calculation, (c) LOD calculation, depicting quenching of [1] on addition of Cu^{2+} ion.

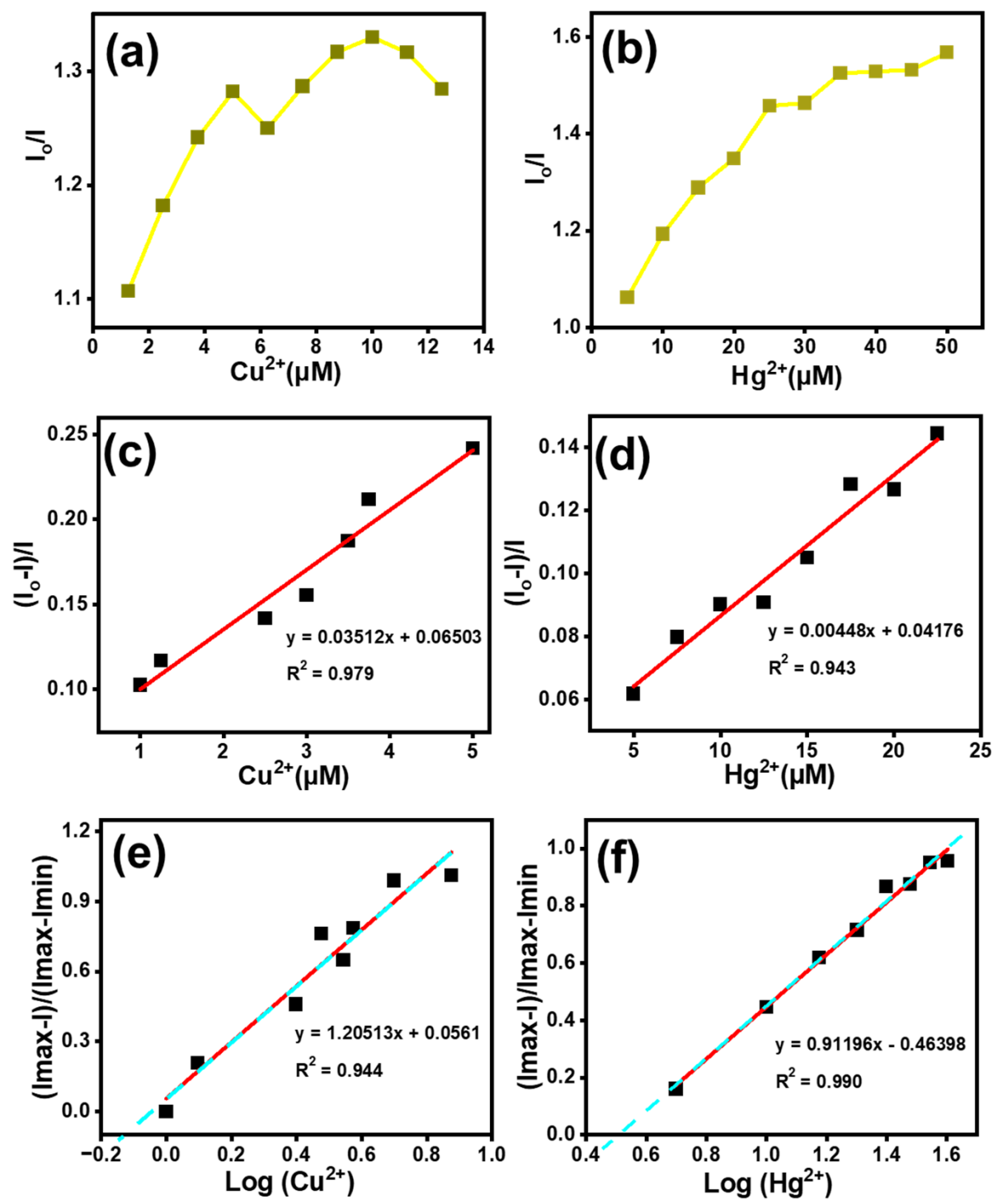


Fig. S10 Stern-Volmer plots for (a) Cu^{2+} and (b) Hg^{2+} , K_{SV} calculation (c) Cu^{2+} and (d) Hg^{2+} , LOD calculation (e) Cu^{2+} and (f) Hg^{2+} , depicting quenching of [2] on addition of metal ion.

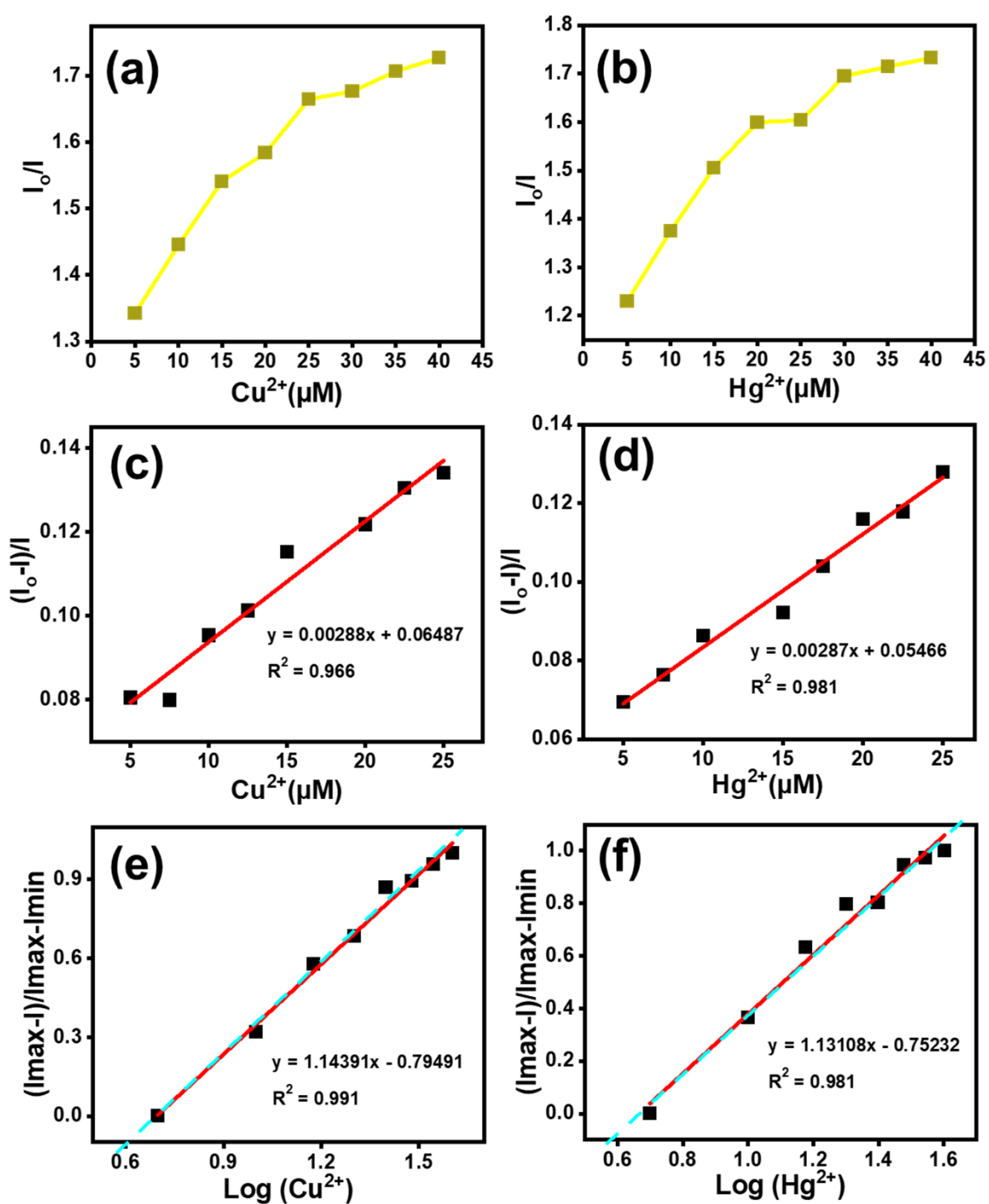


Fig. S11 Stern-Volmer plots for (a) Cu^{2+} and (b) Hg^{2+} , K_{sv} calculation (c) Cu^{2+} and (d) Hg^{2+} , LOD calculation (e) Cu^{2+} and (f) Hg^{2+} depicting quenching of **[3]** on addition of metal ion.

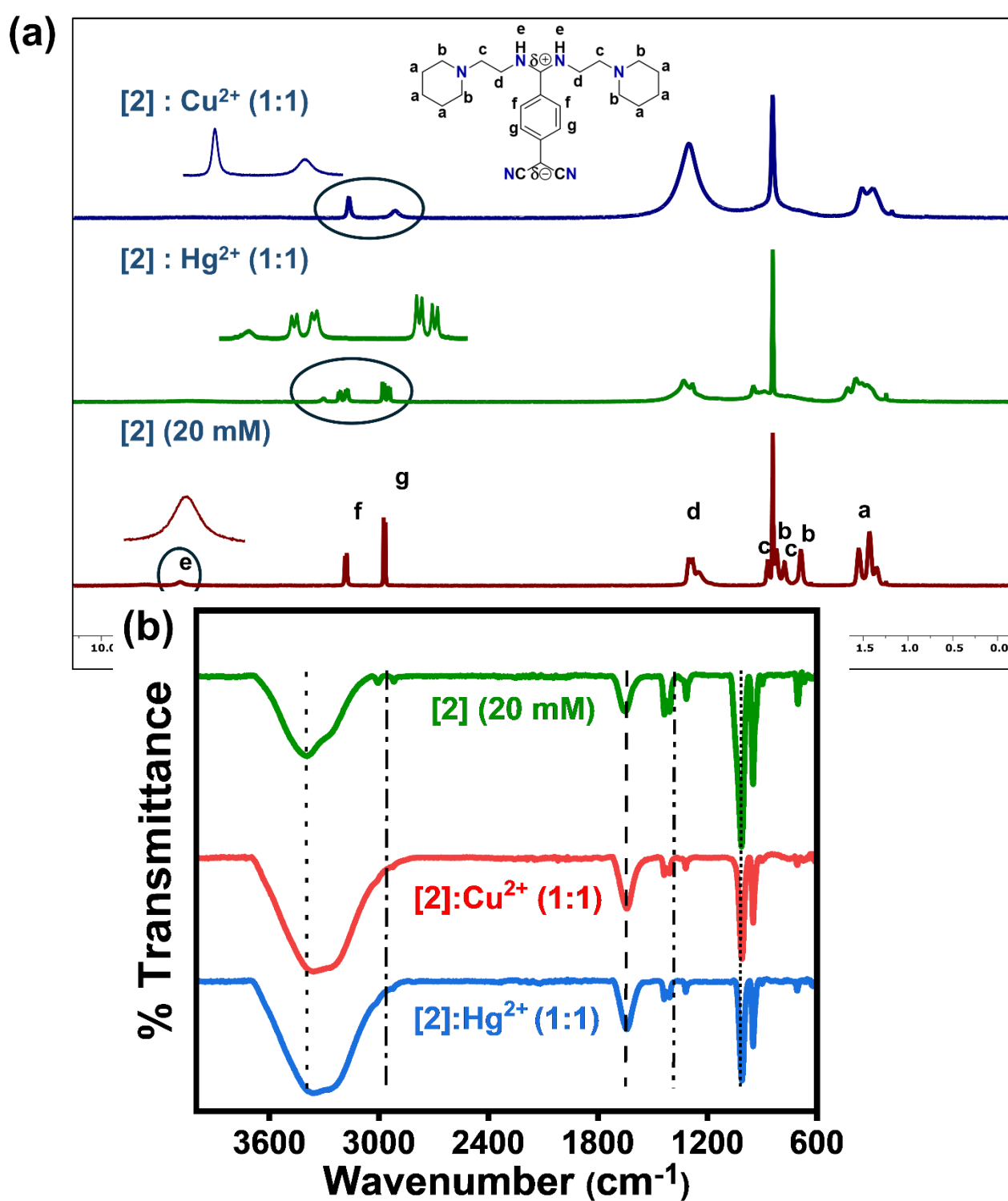


Fig. S12 (a) ^1H NMR to understand the mechanistic insights on addition of metal ions on [2]. (b) FT-IR spectra to understand the mechanistic insights on the addition of metal ions with [2].

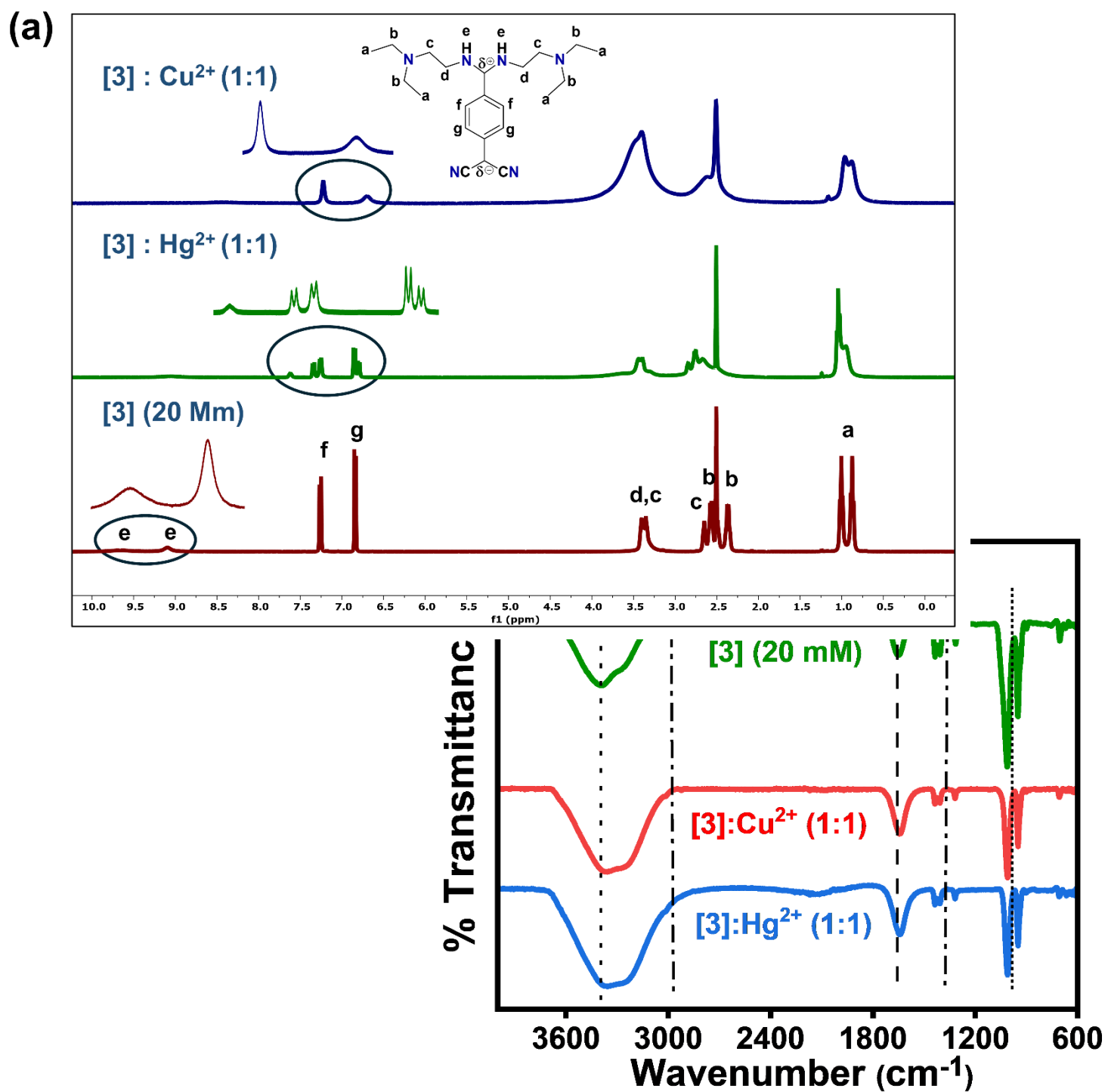
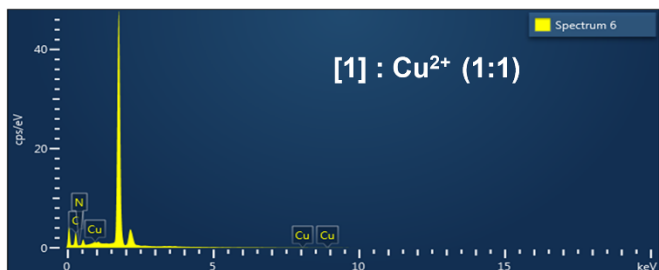


Fig. S13 ^1H NMR to understand the mechanistic insights on addition of metal ions on **[3]**. **(b)** FT-IR spectra showcasing binding of metal ion with **[3]**.

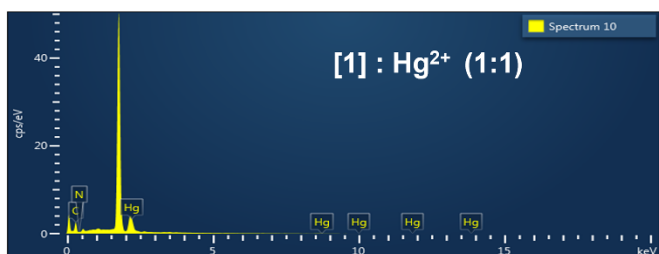
(a)



Element	Wt%	Atomic%
C	71.62	74.63
N	28.38	25.37
Total	100	100



Element	Wt%	Atomic%
C	74.96	79.50
N	21.84	19.86
Cu	3.20	0.64
Total	100	100



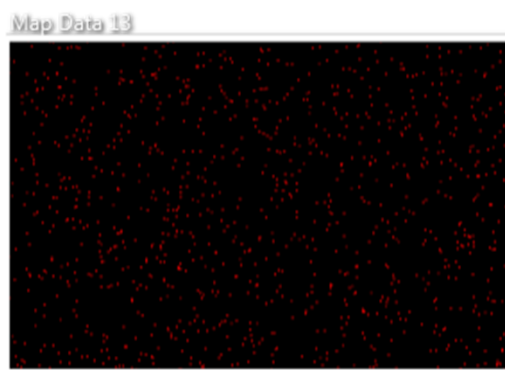
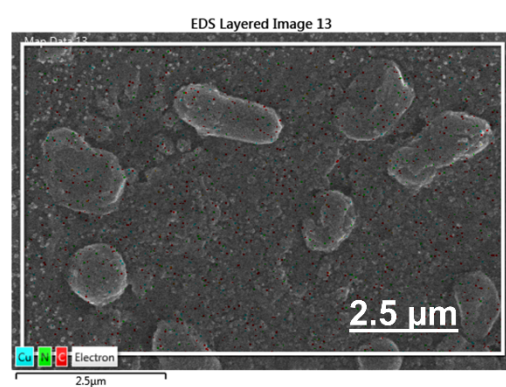
Element	Wt%	Atomic%
C	64.43	88.28
N	8.06	9.47
Hg	27.51	2.26
Total	100	100

16

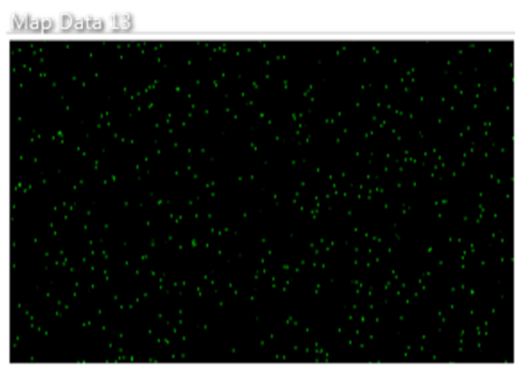
(b)

[1] : Cu^{2+} (1:1)

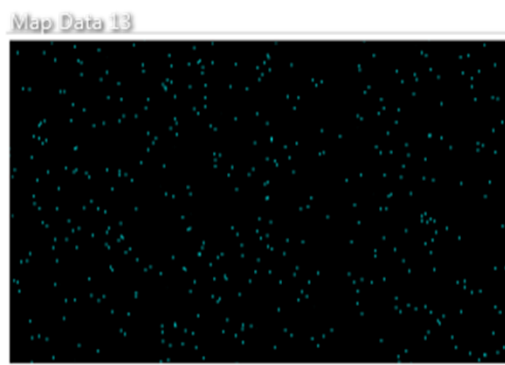
C $\text{K}\alpha_{1,2}$



N $\text{K}\alpha_{1,2}$

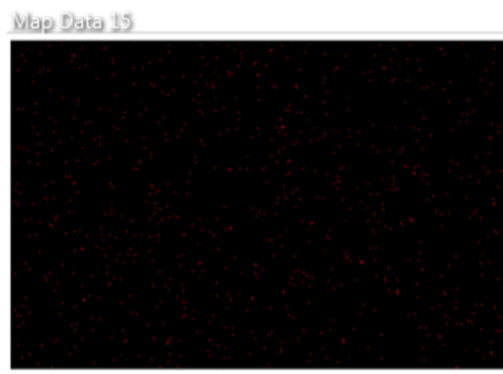
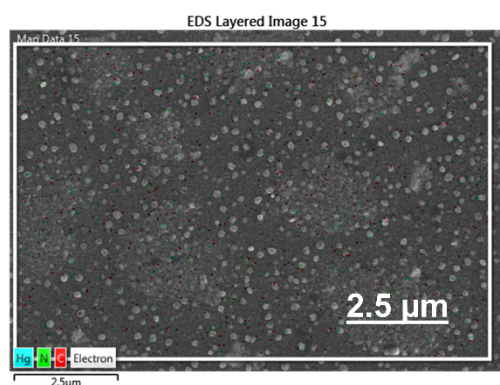


Cu $\text{K}\alpha_1$



[1] : Hg²⁺ (1:1)

C Kα1_2



N Kα1_2

Hg Mα1

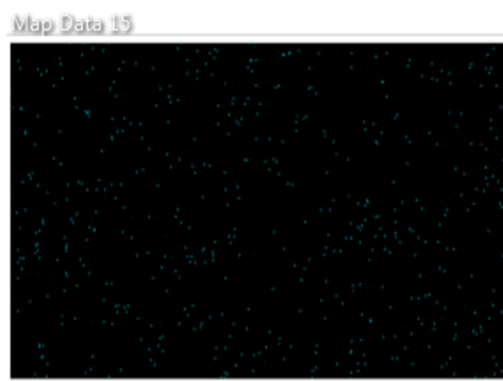
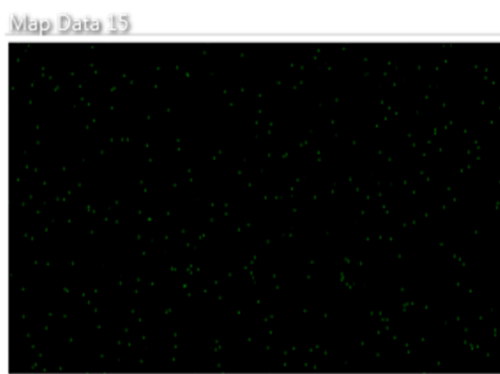
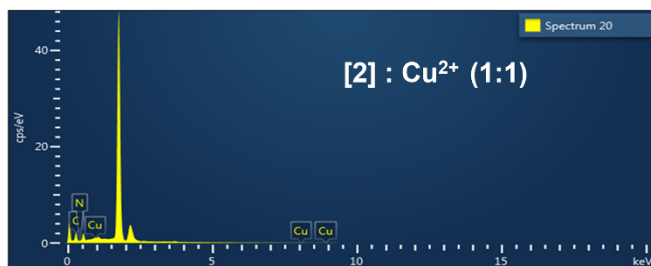


Fig. S14 (a) EDAX spectra showing change in elemental composition for **[1]** with addition of metal ion. (b) EDAX mapping depicting elemental presence for **[1]** on metal ion addition.

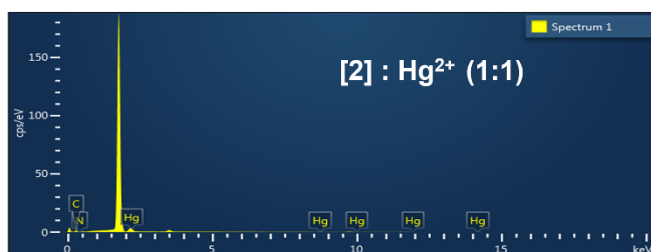
(a)



Element	Wt%	Atomic%
C	68.43	71.66
N	31.57	28.34
Total	100	100



Element	Wt%	Atomic%
C	63.69	68.13
N	34.31	31.47
Cu	2.00	0.41
Total	100	100

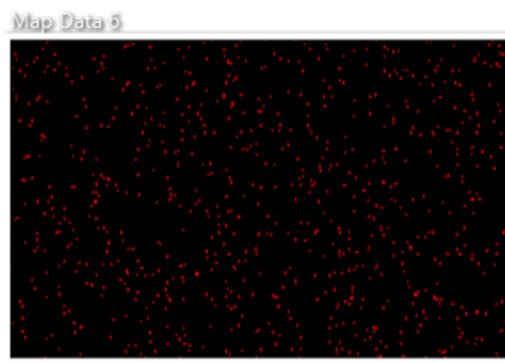
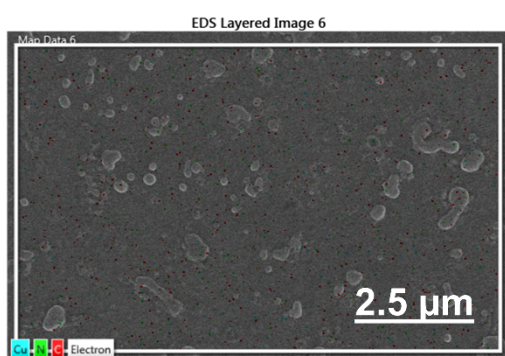


Element	Wt%	Atomic%
C	78.85	95.02
N	3.60	3.72
Hg	17.56	1.27
Total	100	100

(b)

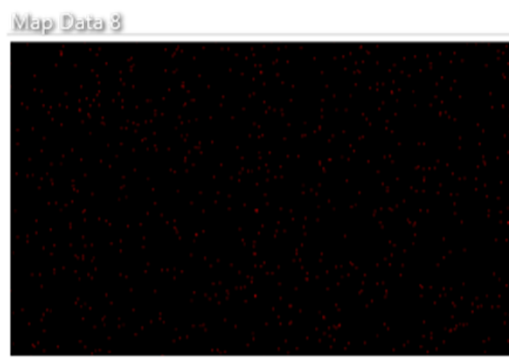
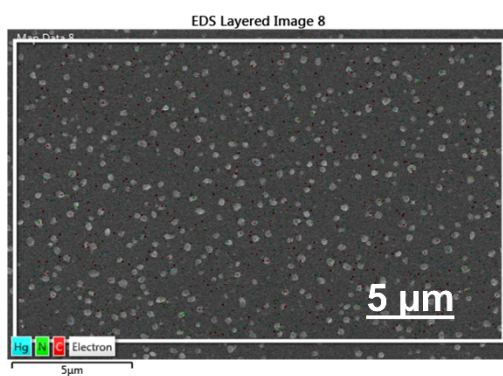
[2] : Cu^{2+} (1:1)

C K α 1_2



[2] : Hg^{2+} (1:1)

C K α 1_2



N K α 1_2

Hg M α 1

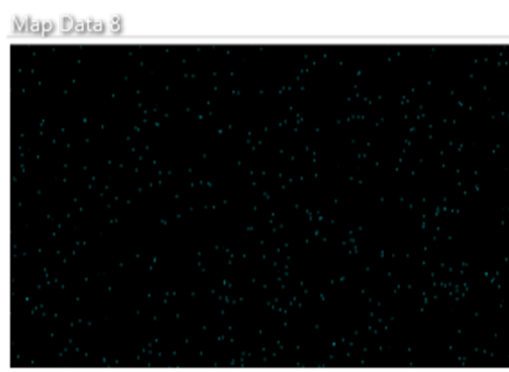
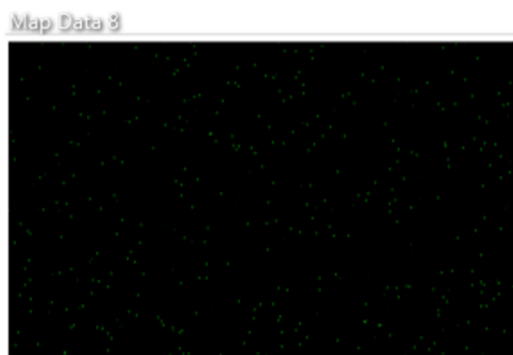
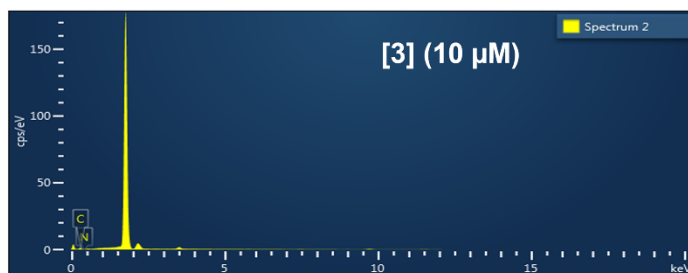
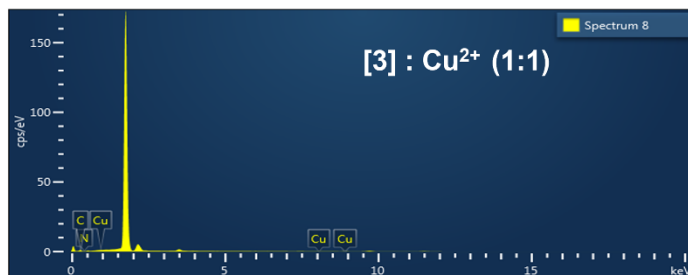


Fig. S15 (a) EDAX spectra showing change in elemental composition for **[2]** with addition of metal ion. (b) EDAX mapping depicting elemental presence for **[2]** on metal ion addition.

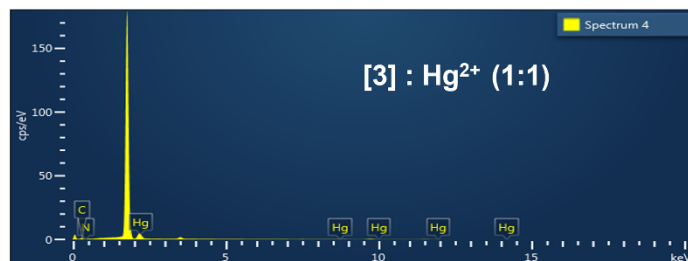
(a)



Element	Wt%	Atomic%
C	69.29	72.46
N	30.71	27.54
Total	100	100



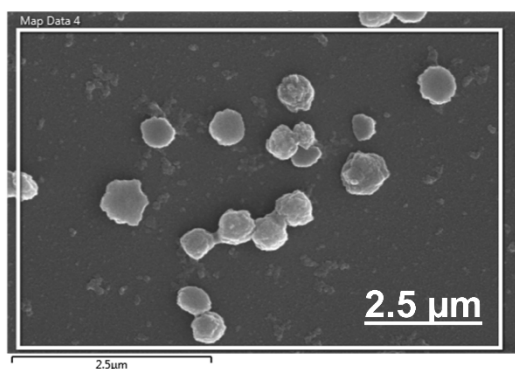
Element	Wt%	Atomic%
C	73.94	79.07
N	21.92	20.09
Cu	4.14	0.84
Total	100	100



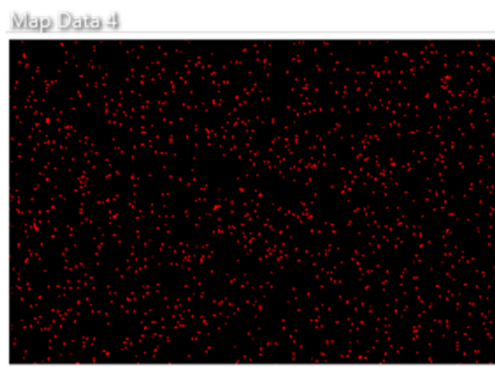
Element	Wt%	Atomic%
C	68.74	88.92
N	8.40	9.31
Hg	22.87	1.77
Total	100	100

(b)

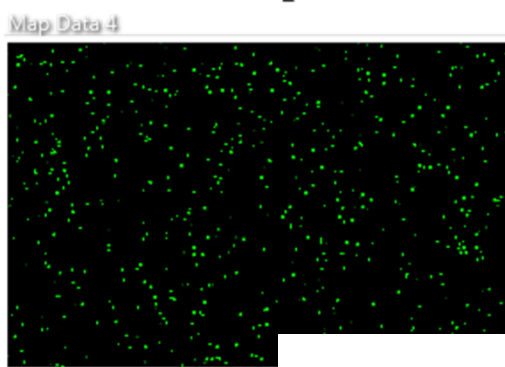
[3] : Cu^{2+} (1:1)



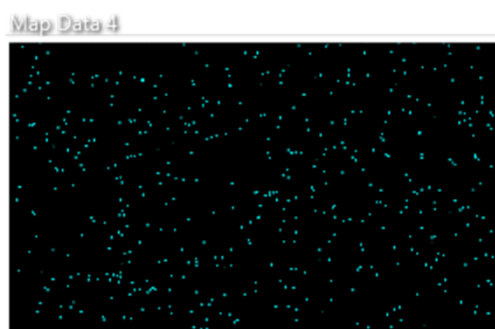
C K α 1_2



N K α 1_2

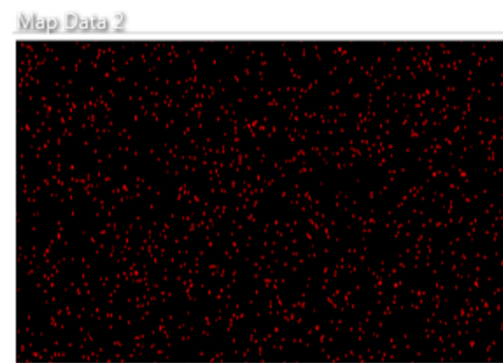
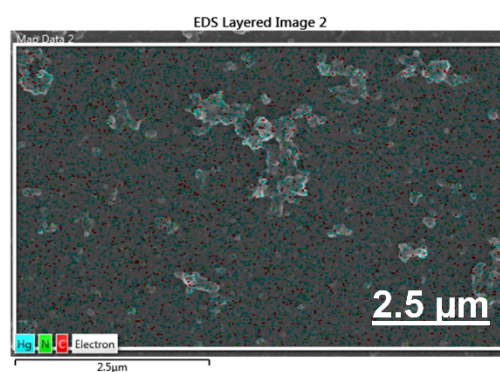


Cu K α 1

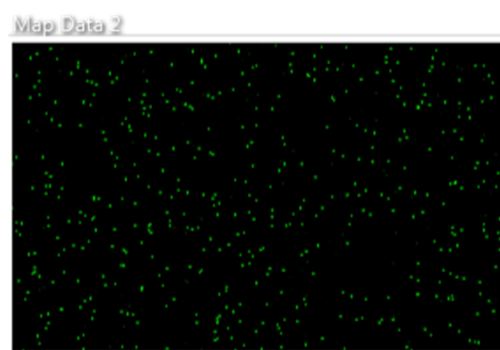


[3] : Hg^{2+} (1:1)

C K α 1_2



N K α 1_2



Hg M α 1

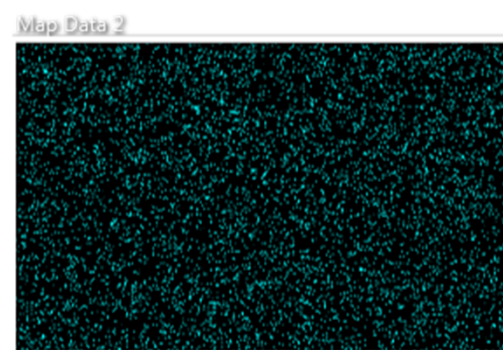


Fig. S16 (a) EDAX spectra showing change in elemental composition for [3] with addition of metal ion. (b) EDAX mapping depicting elemental presence for [3] on metal ion addition.

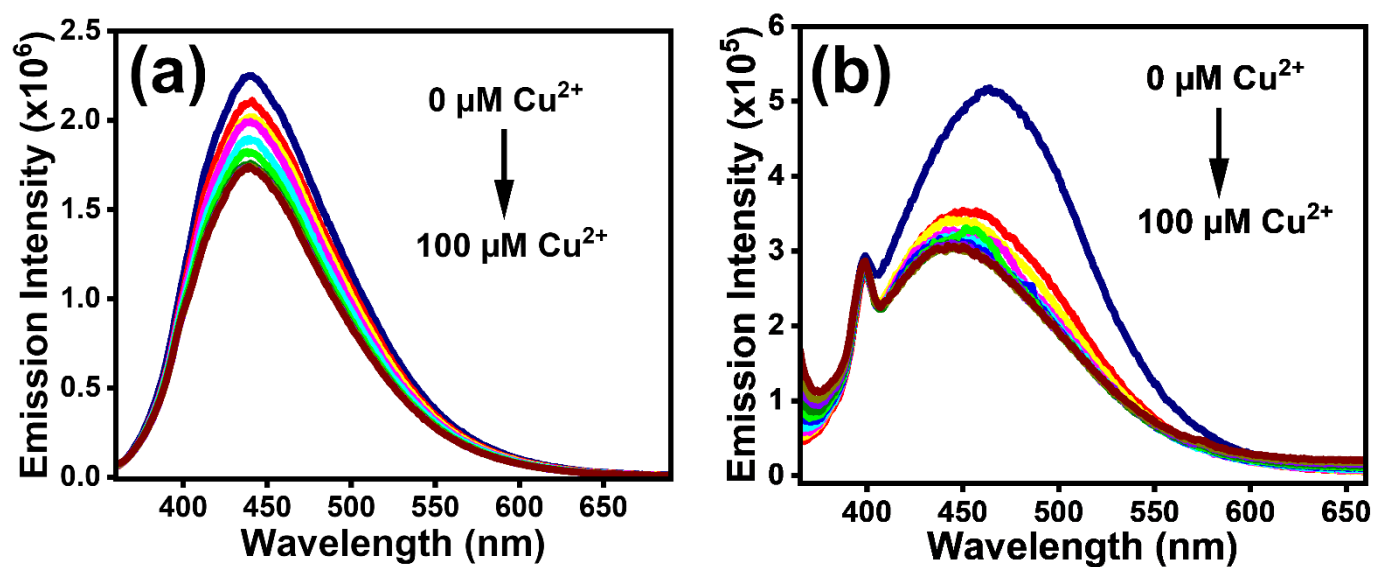


Fig. S17 Variation in emission intensity of [1] against Cu^{2+} ions with (a) pond water sample and (b) tap water sample.